Defence Science Journal, Vol. 67, No. 1, January 2017, pp. 19-25, DOI : 10.14429/dsj.67.10170

Investigation of Stick Propellant Internal Perforation Erosive Burning on Interior Ballistics Performances

Xiaoliang Zhao and Xiaobing Zhang*

Nanjing University of Science and Technology, School of Energy and Power Engineering, China
**E-mail: zhangxb680504@163.com*

ABSTRACT

In this study, a thorough investigation of a stick propellant internal perforation erosive burning on interior ballistic performances is presented via extending the previous work of author. The stick propellant combustion process and the internal perforation erosive burning are revealed by numerical simulations. Different factors with respect to the stick propellant, including propellant length, internal perforation diameter and loading density are analysed in detail. Stick propellant length and the internal perforation diameter have a significant influence on the ballistic performance, the longer and smaller internal propellant have a greater erosive burning effect to the ballistic performance. Loading density has very weak influence on the ballistic.

Keywords: Stick propellant; Erosive burning; Interior ballistics; Propellant length; Internal perforation diameter; Loading density

NOMENCLATURE

E	Internal energy
$2e_1$	Web thickness
f	Propellant force
g	Essential ratio of mass flux
G	Mass flux through the port
l	Propellant travel length
n	Pressure index
p	Average pressure after projectile
r_0	Basic burning rate
S_p	External and end face propellant area
u_1	Burning coefficient
v	Projectile velocity
V_0	Initial chamber volume
V_l	Projectile movement additional volume
V_p	Propellant volume
Z	Relative burned thickness
ρ_p	Propellant density
α	Propellant gas co-volume
ε	Erosive burning coefficient
φ	Minor work coefficient
ψ	Burned propellant fraction
ρ	Gas density
ω_g	Propellant gas mass
λ μ	Sharpe function parameter

1. INTRODUCTION

Compared with the conventional randomly packed grain charge, a stick propellant charge system has some advantages in higher loading density, better flame-spreading and lower pressure waves. Some research groups[2-5] have carried out studies on unslotted stick propellant interior ballistics, they found that the unslotted stick propellant burning rate is higher than that of the granular propellant due to erosive burning, and the overlarge pressure and the rapid pressurisation rate could lead to the grains shattering into small pieces. Yang[6] carried out closed and interrupted bomb tests to study the propellant combustion characters, but its internal perforation flow field can not be revealed. Recently, some researchers[7-10] studied the grain or stick propellant charge interior ballistics performance by the numerical methods, but the erosive burning is not considered. Several researchers[11-16] have presented mechanisms to explain erosive burning phenomenon, such as the flat-plate type scaling of the heat transfer, the compressibility effects and the turbulence effects in semi-empirical treatments. Time-accurate CFD simulations can reveal the flow field detail in the near propellant region, but the high calculation cost leads to the hard application in the real weapon calculation. Mukuna and Paul[17] found out a relatively simple non-dimensional relationship between the ratio of the actual to non-erosive burning rate that matched well with the experiments.

In this study, a fully investigation of the erosive burning influences on ballistic performance of different loading densities and the propellant geometry is carried out under our previous established theoretical work[1]. Different factors, such as propellant length, internal perforation diameter and loading density have been considered in the present work. The gun interior ballistic process of this ballistic model consists of two stages: the stick propellant unbroken stage and the broken stage. The first unbroken stage model has three computational regions, including the solid propellant region, the external lumped parameter region and the internal perforation gas region. In the

Received : 08 June 2016, Revised : 07 November 2016
Accepted : 02 December 2016, Online published : 22 December 2016

internal gas region, a two-dimensional axisymmetric model is simulated and coupled with the solid propellant combustion boundary and the volume increase because of the projectile moving and the propellant combustion. The second broken stage is retrograde into a classical lumped parameter ballistic model.

2. INTERIOR BALLISTIC MODEL ASSUMPTIONS

In the first unbroken stage model, the internal perforation gas region mass injection diagram and detailed calculation flow chart are shown as Fig. 1. The gas region is a two-dimensional axisymmetric, symmetry and inviscid, the gas mass and energy transfer with the external gas region is only through the two side end holes. The propellant gas releases in the very thin layer and the chemical reaction is ignored. The external gas region is a lumped parameter region, the stick propellant external surface combustion gas adds into the external region, and the burning rate depends on the average pressure. The solid propellant is unbroken, rupture or fracture is assumed not exiting in the combustion, and the external diameter releases the energy to the gas region. The second broken stage, the burned propellant fraction and burning surface are introduced to describe the propellant gas generation rate. Propellant burning rate is depended on the chamber average pressure, and the unburned propellant is treated as long cylindrical propellant regressive burning process.

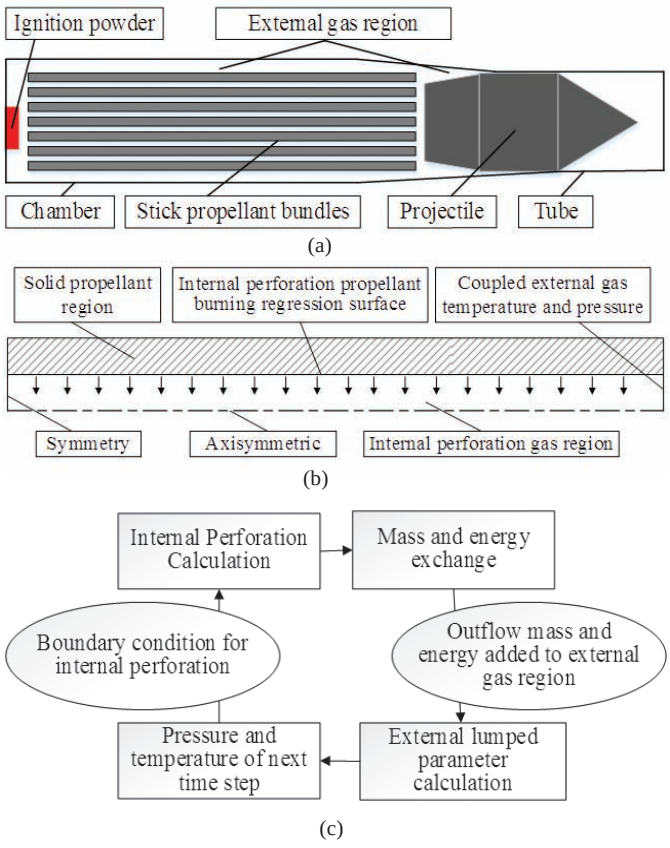

Figure 1. (a) Schematic illustration of stick propellant charge, (b) Diagram of internal perforation mass injection process, and (c) Calculation flow chart of the interior ballistics.

3. MATHEMATICAL MODEL

To better understand the factors influenced the performance of the interior ballistic and the completeness of this work, the model proposed by Zhao & Zhang[1] is summarised as follows.

3.1 The First Propellant Unbroken Stage

External surface burning rate:

$$r_0 = u_1 p^n \tag{1}$$

The mass equation ω_g consists of main three parts,

$$\omega_g = \omega_{flow} + \omega_{out} + \omega_{ign} \tag{2}$$

$$\frac{\mathrm{d}\omega_{out}}{\mathrm{dt}} = \rho_p S_p r_0 \tag{3}$$

Projection motion equation

$$Sp = \varphi m \frac{\mathrm{d}v}{\mathrm{d}t} \tag{4}$$

Travel equation

$$v = \frac{\mathrm{d}l}{\mathrm{d}t} \tag{5}$$

Average gas pressure equation

$$p = \frac{f(\omega_{flow} + \omega_{out}) + \omega_{ign} f_{ign} - \frac{\theta}{2}\varphi m v^2}{\left(V_l + V_0 - V_p - \alpha\omega_g\right)} \tag{6}$$

In the perforation gas region, ignoring the gas viscidity, the two-dimensional compressible flow equations with side mass injection conservative equations are as follows:

$$\frac{\partial Q}{\partial t} + \frac{\partial E}{\partial x} + \frac{\partial F}{\partial y} = 0 \tag{7}$$

where

$$Q = [\rho, \rho u, \rho v, \rho T]^T$$

$$E = [\rho u, \rho u^2 + p, \rho uv, (\rho E + p)u]^T$$

$$F = [\rho v, \rho uv, \rho v^2 + p, (\rho E + p)u]^T$$

Internal propellant mass injection boundary, mass flux is as follow:

$$\dot{m} = \dot{r}\rho_p \tag{8}$$

In the long stick propellant internal combustion, a non-dimensional erosive model is used, and the details are shown by Mukunda & Paul[17].

$$\dot{r} = \varepsilon r_0 \tag{9}$$

$$\varepsilon = 1 + 0.023\left(g^{0.8} - g_{th}^{0.8}\right)\mathrm{H}\left(g - g_{th}\right) \tag{10}$$

$$g = \left(G / \rho_p r_0\right)\left(\rho_p r_0 d_0 / \mu\right)^{-0.125} \tag{11}$$

Mesh motion

The mass inlet boundary grid moving is coupled with the local propellant burning rate, and the grid moves only in the radial direction.

$$y_{new} = y_{old} + \dot{r}\delta t \tag{12}$$

The Euler equations for compressible flow on a moving grid can be written as

$$\frac{\partial}{\partial t}\int_\Omega \rho\phi \mathrm{d}\Omega + \int \rho\phi\left(V - V_g\right)\cdot n\mathrm{d}s = \int_\Omega S_\phi \mathrm{d}\Omega \tag{13}$$

where V_g is the grid moving velocity, V is the gas velocity normal vector.

3.2 The Second Propellant Broken Stage

In this stage, the shape function and the burned fraction web thickness is introduced, projection motion equation and travel equation are same as the previous stage[18]. The equations are as follows:

$$\psi = \begin{cases} Z\left(1+\lambda Z+\mu Z^2\right) & Z \le 1 \\ 1 & Z > 1 \end{cases} \tag{14}$$

$$\frac{\mathrm{d}Z}{\mathrm{d}t} = \frac{u_1 p^n}{e_1} \tag{15}$$

$$p\left(\frac{V_l + V_0}{\omega} - \frac{(1-\psi)}{\rho_p} - \alpha\psi\right) = f\psi - \frac{\theta}{2}\varphi m v^2 \tag{16}$$

4. NUMERICAL APPROACHES

For the external gas lumped parameters region, the first order ordinary differential equations are solved by Runge-Kutta method. Inviscid compressible two dimensional axisymmetric Euler equations, ROE-FDS, i.e. flux-difference splitting approach is applied to the convection flux discretisation. The second order upwind scheme for the flow and squares cell base for the gradient are used for the spatial discretisation. The two dimensional unstructured grids are employed; the propellant surface moves back the calculation region and mesh size increase as propellant burns. The whole system is calculated by FLUENT with a user defined function (UDF) until the propellant burns out.

5. CALCULATION RESULTS AND DISCUSSION

5.1 Validation of the Erosive Model in Closed Bomb Combustion

To validate the Mukuna and Paul[17] non-dimensional erosive model can describe the long stick propellant combustion. The single-perforation stick solid propellant combustion process in the interrupted closed bomb Yang[6] is simulated. The experiment interrupted pressure is approximately 45 MPa controlled by the copper thickness. Figure 2 shows the perforation radius distributions of the calculated results of the relative burning volume in 0.05 to 0.20, and the external average pressure is 45 MPa as the propellant burned fraction is 0.20. The simulated results are in good agreement with the experimental results.

5.2 Ballistic Simulation Result of the Stick Propellant Combustion

The gun and propellant geometry structures are shown in Table 1. The first unbroken erosive burning stage is calculated until the propellant burned fraction to 0.85.

The simulation and experiment results are shown in Table 2, the results show the pressure and muzzle velocity are in good agreement, the relative error is 0.49 per cent and 1.5 per cent. The simulation results are in good agreement in the experiments results.

Table 3 gives the results in different interior ballistics model. The non-erosive burning maximum breech pressure is 288.7 MPa, while the erosive model maximum is 326.6MPa, the pressure relative error is 11.3 per cent; for muzzle velocity, the absolute velocity difference is 52.2 m/s, and the velocity relative error is 5.71 per cent. Compared with the experiment and this paper model results, the differences are large, which means the erosive burning's influence could not be ignored. Here, the total erosive burning coefficient (TEBC) is introduced to describe the erosive burning intensity. The calculation results by increase TEBC to 1.084, the breach pressure and the muzzle velocity are in good agreement with this paper model results.

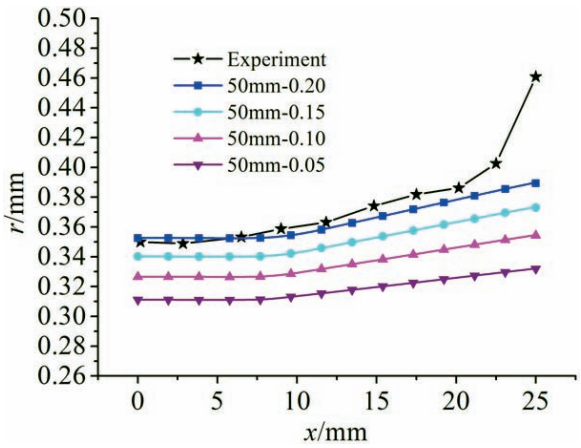

Figure 2. Comparisons of internal perforation radius between the experiment and simulation.

Table 1. Parameters of interior ballistic

Parameter	Value	Parameter	Value
Gun caliber d (mm)	100	Barrel length l(m)	4.732
Chamber volume V_0(m^3)	0.007741	Projectile mass m(kg)	15.6
Co-volume ratio α (m^3/kg)	0.001	Specific heat ratio γ	1.2
Propellant length 2c(mm)	260	Web thickness $2e_1$(mm)	1.7
Propellant force f(J/kg)	980000	Propellant density ρ_p(kg/m^3)	1680
Burning coefficient u_1($m\cdot s^{-1}Pa^n$)	$1.68e10^{-8}$	Pressure exponent n	0.81

Table 2. Comparison of the simulation and experiment results

Parameter	Experiment	Simulation	Relative error %
Breech pressure (MPa)	325.0	326.6	0.49
Muzzle velocity (m/s)	900.0	913.7	1.5

Table 3. Comparison of the simulation and experiment results

Parameter	p (MPa)	v (m/s)	$u_1 ms^{-1}Pa^n$ x 10^{-8}	ε
This paper model	326.6	913.7	1.68	--
Classical model	288.7	861.5	1.68	
Modified erosive coefficient	325.0	902.6	1.82	1.084

Figure 3 shows the velocity and pressure distributions at the burned propellant fraction of 0.3, from the center symmetry face to the end face, the velocity value increases from zero to the maximum value, while the maximum pressure is located at the center symmetry face.

Figure 4 gives the end face maximum gas velocity versus the propellant burned fraction, when $\psi < 0.05$ the gas velocity decreases rapidly and the increase to the maximum value. The pressure difference and gas velocity reaches the maximum value when ψ is near to 0.3. When $\psi > 0.30$ the pressure difference and gas velocity decrease.

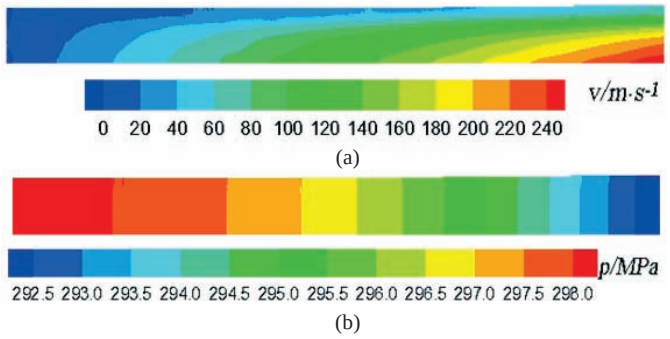

Figure 3. Internal perforation at the burned propellant fraction of 0.3: (a) velocity distribution and (b) pressure distribution.

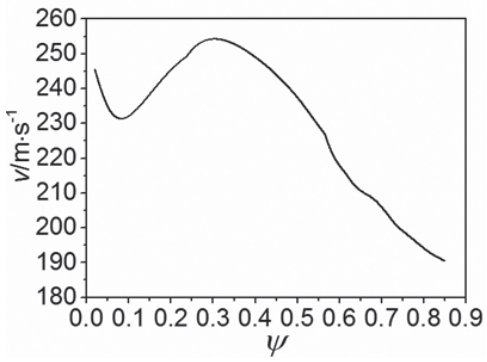

Figure 4. Maximum gas velocity of end face *vs* propellant burned fraction.

6. INFLUENCE OF THE CHARGE PARAMETERS

6.1 Influence of the Propellant Length

Figures 5 and 6 give the end face maximum erosive burning coefficient of different length and the internal and external pressure difference versus propellant burned fraction. In the initial stage, the erosive coefficients decrease rapidly when $\psi < 0.15$, then the erosive coefficient value decreases to a relatively stable level as the propellants burn. The pressure difference tendency is similar to the pressure profile, the pressure difference increases as the local environment pressure increases, the internal gas region release propellant gas is hard to escape to the external gas region. For different length propellants, the long length propellant erosive burning coefficients and the pressure difference are much higher than the short.

Figure 7 shows the erosive burning coefficient value in the axis direction for different propellant length when the burning fraction is 0.3. The erosive burning occurs at the location about 70 mm for the different length, and the erosive coefficient increases when it is closer to the end face. Figure 8 shows the propellant internal radius in the axis direction; the erosive burning speeds up the propellant combustion rate.

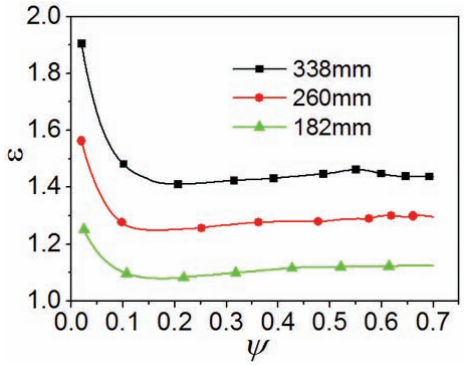

Figure 5. End face maximum erosive coefficient versus propellant burned fraction of different length.

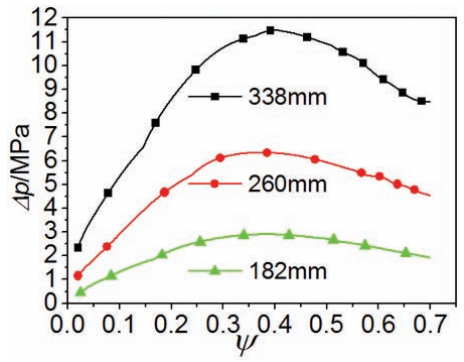

Figure 6. Maximum pressure difference versus propellant burned fraction of different length.

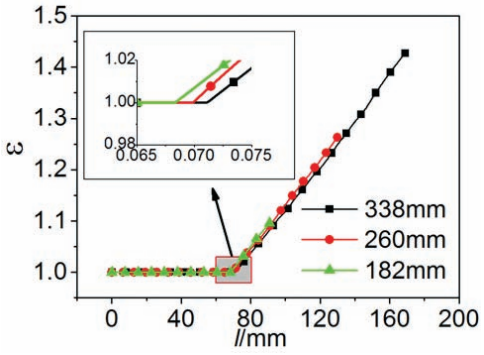

Figure 7. Erosive burning coefficient distribution when the burned fraction is 0.3.

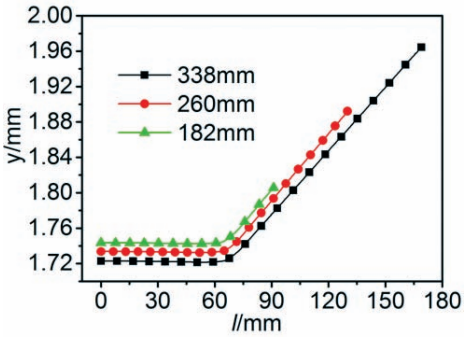

Figure 8. Internal radius distribution burned fraction is 0.3 in different length.

Figure 9 shows the TEBC of different lengths, 1.117, 1.084, and 1.055, respectively. The erosive burning coefficient increases rapidly with the increase of propellant length increase, which is caused by both the larger erosive burning area the higher erosive burning intensity.

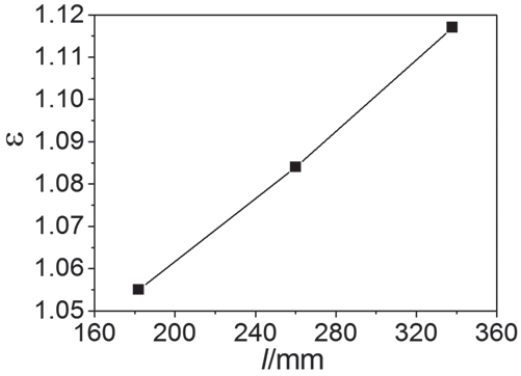

Figure 9. Modified erosive burning coefficient of different propellant length.

6.2 Influence of the Propellant Internal Diameter

Propellant internal diameter is a vital factor for the propellant length to diameter ratio, the propellant end face erosive burning coefficients are as shown in Figs. 10, 11, and 12. The initial end faces erosive coefficient for the 1.77 mm diameter propellant is higher than the large case, the 3.29 mm diameter propellant erosive burning coefficient is closed to 1, which means the erosive burning has very weakly influence. The small diameter propellant pressure difference is much

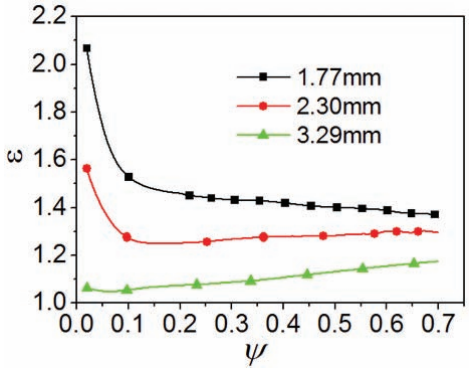

Figure 10. Maximum erosive coefficient of end face *vs* propellant burned fraction of different radius.

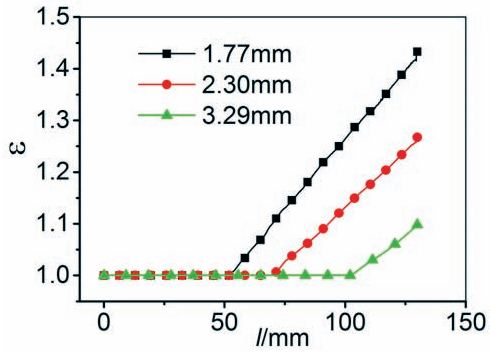

Figure 11. Erosive burning coefficient distribution when the burned fraction is 0.3 in different diameters.

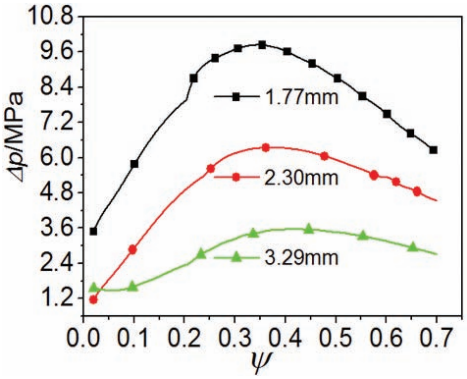

Figure 12. Maximum pressure difference *vs* propellant burned fraction of different radius.

higher than the large, the propellant in the small diameter perforation is hard to escape from the end face perforation, so the pressure difference is higher than the large. Fig. 13 shows the modified erosive coefficients of different lengths. The TEBC decreases rapidly with the increase of propellant internal perforation diameter.

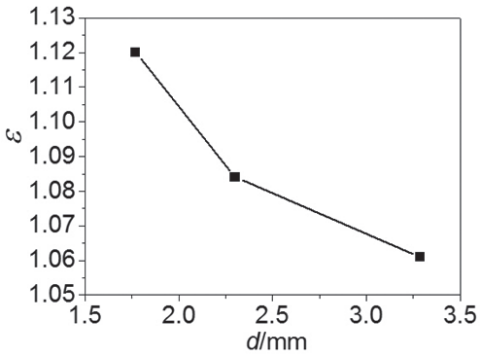

Figure 13. Modified erosive burning coefficient of different internal diameter.

6.3 Influence of Different Charge Loading Density

Figures 14 and 15 show the end face maximum erosive burning coefficient of different loading densities and the internal and external pressure difference versus propellant burned fraction. The 3.73 kg and 4.20 kg erosive burning coefficient curves are almost coincident and decrease rapidly when $\psi < 0.10$, but the two values are larger than the 5.60kg propellant charge. The 5.60 kg loading propellant charge pressure is much higher than the lower loading charge.

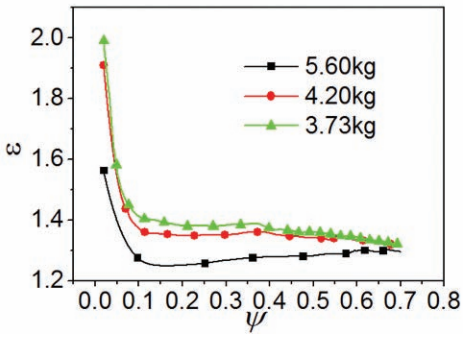

Figure 14. Maximum erosive coefficient of end face *vs* propellant burned fraction of different loading density.

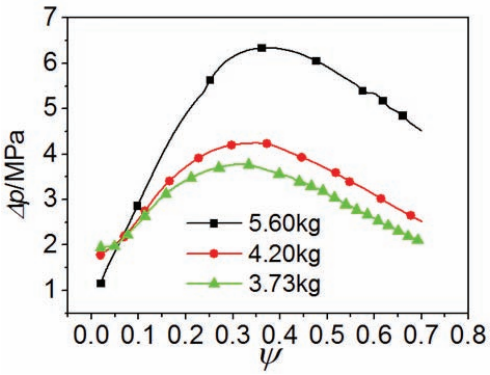

Figure 15. Maximum pressure difference versus propellant burned fraction of different loading density.

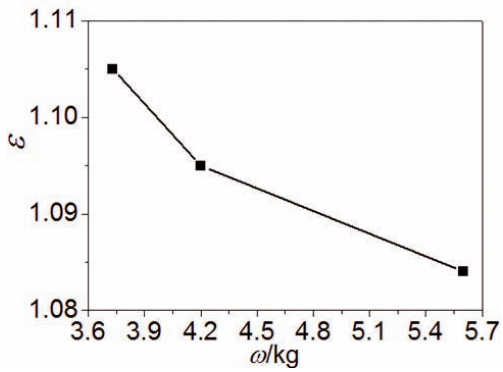

Figure 16. Modified erosive burning coefficient of different loading density.

The erosive burning coefficients increase with increase of the loading density are shown in Fig. 16. The loading density have weak influence compared with the propellant length and the internal perforation diameter.

7. CONCLUSIONS

The results of numerical simulation show that the model in our previous work can describe the single perforation stick propellant interior ballistics by considering the internal perforation erosive burning, and the pressure and velocity time history can be obtained. Erosive burning occurs especially during the initial interior ballistic period and leads to higher peak pressure and muzzle velocity from the perspective of the interior ballistic performance.

In addition, stick propellant length and internal perforation diameter can affect the interior ballistic performance obviously. Pressure difference value decreases obviously as the propellant length decrease. The erosive burning threshold positions of different length are almost at the same position, and the erosive burning coefficient distribution is similar. The total erosive burning modify intensity of long stick propellant is cause by the larger erosive burning area and the higher erosive burning intensity.

The small diameter stick propellant erosive burning threshold position is much closer to the center than the larger diameters. The pressure different and the erosive burning coefficient in the small diameter is larger than the large diameter. The erosive burning phenomenon will disappear when the internal perforation diameter is larger than 3.29 mm.

Erosive burning coefficient in low loading density is larger than the high loading condition, but the loading density influence is very slightly. Pressure difference increases obviously as the loading density increases.

REFERENCES

1. Zhao, X. & Zhang, X. Study of stick-propellant gun interior ballistic considering internal perforation erosive burning. *In* Proceedings - 29th International Symposium on Ballistics, Ballistics 2016, 2016, **1**, pp.880-887.
2. Juhasz, A.A. Effects of perforation L/D ratio and slotting on stick propellant combustion. Army Ballistic Research Lab Aberdeen Proving Ground, MD, 1984. Report No. BRL-TR-2602.
3. Yamada K, Ishikawa N. Simulative study on the erosive burning of solid rocket motors. *AIAA J.* 1976, **14**(9), 1170-1176. doi: 10.2514/3.61451
4. Char, J. M. & Kuo, K.K. Study of combustion processes of single-perforated stick propellants. *J. Propul. Power.* 1989, **5**(3), 262-268. doi:10.2514/3.23147
5. Hsieh, W.H. Erosive and strand burning of stick propellants, Part I. Measurements of burning rates and thermal-wave structures. *J. Propul. Power,* 1990, **6**(4), 392-399. doi:10.2514/3.25448
6. Yang, F. The research of the erosive burning effect on TEGN propellant. Nanjing University of Science and Technology. 2013. (Master thesis, Chinese)
7. Rashad, M.; Zhang, X. & Elsadek, H. Interior ballistic two-phase flow model of guided-projectile gun system utilizing stick propellant charge. *WSEAS Trans. Appl. Theoretical Mech.*, 2014, **9**, 124-135. doi:10.1002/prep.201400034
8. Miura, H. & Matsuo, A. & Nakamura, Y. Numerical prediction of interior ballistics performance of projectile accelerator using granular or tubular solid propellant. *Propellants, Explosives, Pyrot.*, 2013, **38**(2), 204-213. doi:10.2514/6.2010-1145
9. Jang, J.; Oh, S. & Roh, T. Development of three-dimensional numerical model for combustion-flow in interior ballistics. *J. Mech. Sci. Technol.*, 2016, **30**(4), 1631-1637. doi:10.1007/ s12206-016-0319-y
10. Jang, J. Numerical analysis of interior ballistics through Eulerian-lagrangian approach. *J. Mech. Sci. Technol.*, 2013, **27**(8), 2351-2357. doi: 10.1007/s12206-013-0619-4
11. Lenoir, J. M. and G. Robillard. A mathematical method to predict the effects of erosive burning in solid-propellant rockets. *Symposium Combustion*, 1957, **6**(1), 663-667. doi:10.1016/S0082-0784(57)80092-7
12. Green, L. Erosive burning of some composite solid propellants. *J. Jet Propulsion*, 1954, **24**(1), 8-15. doi: 10.2514/8.6439
13. Razdan, M. & Kuo, K. Erosive burning study of composite solid propellants by turbulent boundary-layer approach. *AIAA* J., 1979, **17**(11), 1225-1233. doi: 10.2514/6.1978-978
14. Mcdonald, B.A. & Menon, S. Direct numerical simulation

of solid propellant combustion in crossflow. *J. Propul Power*, 2005, **21**(3), 460-469. doi:10.2514/1.10049
15. Zhang, J. & Jackson, T.L. A model for erosive burning of homogeneous propellants. *Combustion Flame*, 2010, **157**(2), 397-407. doi: 10.1016/j.combustflame.2009.09.0 08
16. Jackson, T.L. Modeling of heterogeneous propellant combustion: A survey. *AIAA J.*, 2012, **50**(50), 993-1006. doi:10.2514/1. J051585
17. Mukunda, S.H. & Paul, J.P. Universal behaviour in erosive burning of solid propellants. *Combustion Flame*, 1997, **109**(1-2), 224-236. doi: 10.1016/S00102180 (96)00150-2
18. Zhi-ming, Jin. Interior ballistics of guns. Beijing: Beijing Institute of Technology Press. 2007.

ACKNOWLEDGMENTS

This work is supported by the Natural Science Foundation of Jiangsu Province (Grant No. BK20131348) and Key Laboratory Foundation of the People's Republic of China (Grant No. 9140C300206120C30110), the National Natural Science Foundation of China (Grant No. 11502114), China Postdoctoral Science Foundation funded project (Grant No. 2015M581797).

CONTRIBUTORS

Mr Xiaoliang Zhao received the BS in the School of the Energy and Power Engineering from Nanjing University of Science and Technology, Nanjing, Jiangsu, China, in 2007. He is working towards the PhD in the School of the Energy and Power Engineering from Nanjing University of Science and Technology. His research interests are interior ballistics of guns.

In this study, he proposed the interior ballistic model of this paper, did the coding and carried out the simulations in different conditions to reveal the erosive burning effects to the ballistics performances.

Dr Xiaobing Zhang received the BS, MS, and PhD in the School of the Energy and Power Engineering from Nanjing University of Science and Technology, Nanjing, Jiangsu, China, in 1990, 1992, and 1995, respectively. Currently he is the professor in Nanjing University of Science and Technology. His research interests are the interior ballistics of guns, heat transfer and fluid mechanics.

In this study, he has done the overall planning and the guidance of the work, review of the simulation results and give the modification for the final manuscript.